Available online at www.sciencedirect.com
ScienceDirect
Catalysis Today 123 (2007) 50–58
CATALYSIS TODAY
www.elsevier.com/locate/cattod

The effect of mesoporous scale defects on the activity of Au/TS-1 for the epoxidation of propylene

Bradley Taylor [a], Jochen Lauterbach [b], W. Nicholas Delgass [c,*]

[a] Advanced Hydrocarbon Fuels, Bartlesville Technology Center, ConocoPhillips, Bartlesville, OK 74004, USA
[b] Department of Chemical Engineering, University of Delaware, Newark, DE 19716, USA
[c] Forney Hall of Chemical Engineering, Purdue University, 480 Stadium Mall Drive, West Lafayette, IN 47907-2100, USA

Available online 14 January 2007

Abstract

In an effort to examine the role of crystal morphology on activity, mesoporous scale defects were introduced into titanium silicalite-1 (TS-1) support materials through the addition of carbon pearls during the synthesis procedure. Catalysts prepared using these support materials were consistently active and stable, with a 0.33 wt% Au catalyst producing 132 $g_{PO}/h/kg_{cat}$ at 200 °C, the highest propylene oxide (PO) rate thus reported, despite relatively high gold loadings and considerable contamination with octahedral titanium species. While activity is high per gram catalyst, activity per gram gold was still relatively low implying that a significant portion of gold deposited on the support surface may be inactive for epoxidation.

Keywords: Mesoporous catalysts; Propylene; Epoxidation; Au catalysts; TS-1

1. Introduction

Since the discovery in 1998 of the propylene epoxidation activity of the Au–Ti system in the presence of hydrogen and oxygen [1], considerable effort has been made to produce materials that overcome the limited rates and stability of early gold on anatase catalysts. Although any number of methods for producing an Au–Ti interface has resulted in some epoxidation activity [2,3], deposition precipitation (DP) was undeniably shown to most efficiently produce the necessary Au–Ti interaction [1–3]. While refinement of the DP method increased the epoxidation rate over these catalysts [4,5], stability remained poor. Catalysts prepared by DP onto anatase supports were found to deactivate primarily through the further reaction of propylene oxide (PO) with titanium adjacent to the Au–Ti interface [6]. The detrimental effect of titanium connectivity has since been well established through the examination of titania supported on silica, sub-monolayer titania on silica, and finally titanium inserted into zeolitic frameworks [4,7,8]. The emphasis on catalysts prepared by DP of gold onto isolated titanium containing supports, encouraged by the inherent epoxidation activity of tetrahedrally coordinated titanium for the liquid phase epoxidation reactions [9], has led to a number of state of the art catalysts prepared through the insertion of titanium into nanoporous silicalite frameworks [4,7,8,10–23]. The marrying of nanoscale gold size effects, Au–Ti synergy and nanoporous support materials has resulted in catalysts over an order of magnitude more active [24,25] and in some cases several orders of magnitude more stable [4,5,25] than the pioneering catalysts of this system [1]. The true nature of the active gold species and its interaction with titanium remains unresolved. The work presented here builds on the conclusions previously presented in the literature focusing on the use of a highly dispersed titanium containing support, in this case titanium silicalite-1 (TS-1), onto which gold has been deposited by DP and following up on the qualitative observation in this laboratory that TS-1 particle morphology plays an important role in the observed epoxidation activity. Prismatic crystallites generally resulted in inferior catalysts as compared to materials with more globular or spheroidal particle morphologies. Superior performance from catalysts made from poorly formed TS-1 crystallites implied that structural defects of some kind might play a vital role in the activity of the Au–Ti system. Examination of the epoxidation of propylene by hydrogen peroxide via density functional theory

* Corresponding author. Tel.: +1 765 494 4059; fax: +1 765 494 0805.
E-mail address: delgass@ecn.purdue.edu (W.N. Delgass).

0920-5861/$ – see front matter
doi:10.1016/j.cattod.2007.01.005

calculations (DFT) has shown that while a well-defined tetrahedral titanium center is required for epoxidation to proceed, the energetics of this reaction are vastly improved through the introduction of a silicon vacancy adjacent to a titanium site [26]. In an effort to produce support materials with an enhanced number of titanium/defect pairs, we turned to the introduction of a secondary structure directing agent that was disruptive to crystallite growth. As previously shown in the literature, first using ZSM-5 [27] and subsequently using TS-1 [28], the introduction of 12–20 nm carbon pearls into the zeolite synthesis gel can result in a disordered mesoporosity in otherwise morphologically prismatic crystallites. The adaptation of this method to produce increasingly textured and potentially mesoporous spheroidal TS-1 particle morphologies was used to develop support materials for the gas-phase epoxidation reaction with the potential for an enhanced number of titanium/defect pairs induced by the directed growth of the zeolite around removable nanoscale obstructions. The introduction of a solid secondary structure directing agent allowed the localization of titanium (as was shown previously with aluminum in ZSM-5 [27]) near the external crystallite surface so as to be proximate to gold entities larger than the microporous channel system could accommodate. We report here on a synthesis procedure that consistently results in modified support materials, which, upon desposition of gold, produce catalysts of appreciable activity and considerable stability for the production of PO.

2. Experimental procedures

2.1. Support synthesis

The procedure for the growth of TS-1 in the presence to carbon pearls was adapted from the synthesis as previously published by researchers at the Haldor-Topsøe Company [27,28]. Synthesis began with 6.7 g of carbon pearls (Cabot, Carbon Pearls 2000) that were dried overnight at 160 °C under vacuum. The carbon pearls were then combined drop-wise with approximately 22 mL of tetrapropylammonium hydroxide (TPAOH, Alfa Aesar, 40 wt% in water) to incipient wetness. Immediately following addition of the template, a mixture of 25 mL of tetraethylorthosilicate (TEOS, Aldrich, 98%+), 1.1 mL titanium(IV) butoxide (TBOT, Alfa Aesar, 99%+) and 8 mL of isopropyl alcohol (IPA, Mallinckrodt, ChromAR® HPLC), which corresponds to approximately 15% above incipient wetness, was added to the previously impregnated carbon pearls. Once combined, the synthesis gel and carbon pearls were allowed to age in air at room temperature for 3 h. Following aging, the mixture was placed in a Teflon-lined autoclave, covered with deionized water (approximately 35 mL) to approximately 1 in from the autoclave seal, and heated under autogeneous pressure at 170 °C for 24 h. Following cooling to room temperature, the contents of the autoclave were filtered and washed with approximately 600 mL of deionized water, and placed in a vacuum drying oven at room temperature. Once dry, the black solid was placed in a furnace at room temperature, ramped to 535 °C over the course of 5 h and calcined at 535 °C for at least 10 h in 20 vol% oxygen in helium (50 sccm) in order to remove the templating agent and combust the carbon pearls.

Three TS-1 support materials were prepared via the carbon pearl synthesis route and have been named according to the Si/Ti ratio as shown in Table 1. The prefix PC has been added to the material designation to denote the 'pearly carbon' synthesis route. PCTS-1(27) was prepared identically to the sample preparation presentented above. PCTS-1(28) was prepared similarly to the method presented above, except the titanium precursor was mixed with the templating agent and impregnated onto the carbon pearls, rather than being mixed with the silicon precursor, and added in the second impregnation. PCTS-1(44) was prepared similarly to PCTS-1(28) except only one-half the volume of titanium precursor was used.

2.2. Deposition of gold

Gold was deposited using the method of deposition precipitation as outlined by Tsubota et al. [12]. An appropriate amount of hydrogen tetrachloroaurate(III) ($HAuCl_4{\cdot}xH_2O$, Alfa Aesar, 99.999%) was dissolved in 50 mL of deionized water resulting in the gold solution concentrations found in Table 1. Following suspension of approximately 1 g of calcined support material in the gold precursor solution, the slurry was neutralized to a pH of 9 using a saturated aqueous solution of sodium carbonate. The slurry was allowed to stir for 4 h at room temperature, after which the solid was removed via centrifugation, re-suspended in approximately 50 mL of deionized water, separated again by centrifugation and dried under vacuum at room temperature. In general, less than 2% of the available gold in solution was deposited onto the support material. Catalysts were named for the gold loading and the support material as is shown in Table 1.

3. Catalyst characterization and evaluation

3.1. Catalyst characterization

The bulk structure of the support materials was determined using X-ray diffraction (XRD, Siemens D500 Diffractometer,

Table 1
Summary of the catalysts prepared from support materials synthesized using carbon pearls

Catalyst	Support	Ti loading (wt%)	Si/Ti	Gold content of DP solution (g/L)	Gold loading (wt%)	Gold particle size (nm)
0.03Au/PCTS-1(27)	TS-1 via carbon pearls	2.9	27	1.01	0.03	–
0.33Au/PCTS-1(28)	TS-1 via Ti impregnated carbon pearls	2.8	28	2.56	0.33	3.5 ± 1.4
0.04Au/PCTS-1(44)	TS-1 via Ti impregnated carbon pearls	1.8	44	0.972	0.04	–

Cu Kα). Small angle X-ray scattering (SAXS, Molecular Metrology, BEDE Cu Microsource, Gas-Filled Multiwire Proportional Array Detector) and ultra small angle scattering (USAXS, Molecular Metrology, Cu Kα, Germanium Bonse-Hart Camera) were used to probe for any mesoporosity or long-range order. Support surface areas were estimated using nitrogen absorption isotherms (Micromeretics ASAP 2000). The local environment of the titanium in the support material was evaluated using diffuse reflectance ultraviolet–visible spectroscopy (DRUV–vis, Varian Cary 5000 outfitted with Harrick Praying Mantis optics). Support and gold particle sizes were determined by transmission electron microscopy (TEM, JEOL 2000 FX, 200 keV) and metal loadings were determined using atomic absorption spectroscopy (AAS, Perkin-Elmer AAnalyst 300).

3.2. Kinetic evaluation

Kinetic measurements were obtained using a 0.5-in-diameter steel vertical reactor operating at differential conversion. Catalysts were sieved to 60–80 mesh and evaluated in a reactant mixture consisting of 10/10/10/70 vol% hydrogen (99.999%), oxygen (99.999%), propylene (99.9%) and helium (99.999%) with a total flow rate of 35 sccm and a resulting space velocity of 7000 mL/h/g_{cat}. The effects of deactivation by aging on the shelf were minimized by evaluating catalysts within 24 h of preparation. Each catalyst was evaluated without any pretreatment and activated on stream in the reactant mixture at 200 °C. Each catalyst was evaluated using a four-segment temperature cycle consisting of 12 h at 200 °C followed by 6 h at 140, 200 and 170 °C, each separated by 2 h of temperature ramping. The reactor effluent was separated using a Varian 3700 gas chromatograph. Organic products were separated on a Supelcowax 10 capillary column (0.53 mm × 60 m) and analyzed using a flame ionization detector. Inorganic products were separated on a ChromosorB 102 packed column (1/8 in × 8 ft) and analyzed using a thermo-conductivity detector. Hydrogen efficiency was estimated using the consumption of oxygen during reaction. External mass transfer limitations were eliminated by operating at a high space velocity and internal mass transfer limitations were neglected because the Thiele modulus was estimated to be smaller than 1 (using a diffusion coefficient of 10^{-4} cm^2/s).

4. Results

4.1. Support characterization

The three support samples were examined by XRD to determine the effects of carbon pearls on the growth of the TS-1 crystallites (Fig. 1). The diffraction patterns obtained were consistent with the orthorhombic space group (*Pnma*) for TS-1 as indicated by the lack of splitting of the diffraction peak at approximately 24.7° 2θ using Cu Kα radiation. No significant line broadening was observed as compared to diffraction patterns of materials made using other preparation methods [25]. Examination of the local titanium coordination using

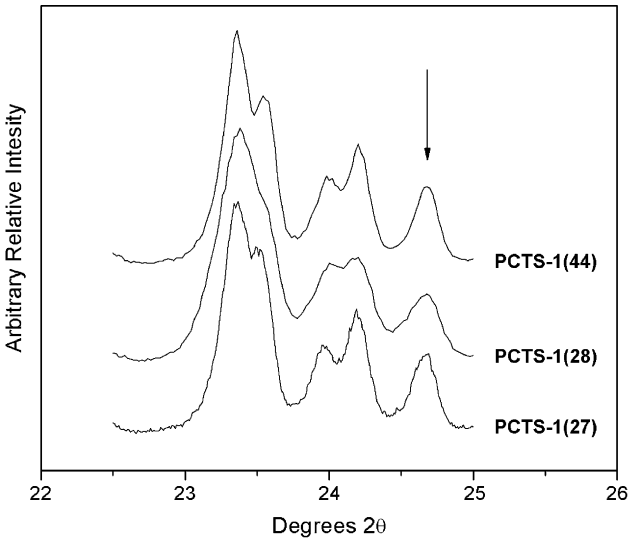

Fig. 1. XRD patterns for the TS-1 supports PCTS-1(27), PCTS-1(28) and PCTS-1(44). The diffraction peak indicated by the arrow at approximately 24.7° 2θ is indicative of the orthorhombic structure generally observed for TS-1.

DRUV–vis revealed a number of local bonding environments in each sample (Fig. 2). PCTS-1(27), the material prepared most similarly to the published procedures [27,28], resulted in a strong peak at 224 nm and high wavelength shoulders at approximately 260 and 300 nm. PCTS-1(28) and PCTS-1(44) were qualitatively similar with main peaks at 220 nm and high wavelength shoulders at approximately 255 nm.

Changes in particle morphology, a primary rationalization of the addition of carbon pearls to the zeolite growth gel, were

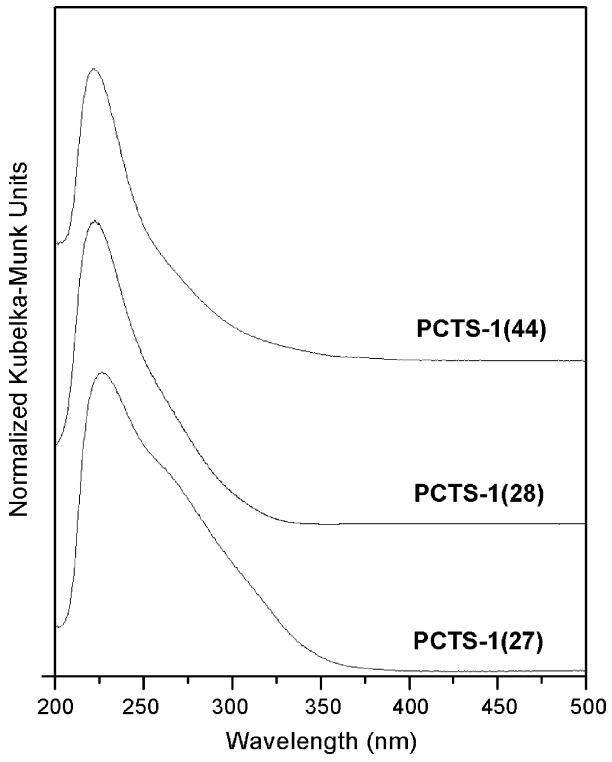

Fig. 2. DRUV–vis spectra for PCTS-1(27), PCTS-1(28) and PCTS-1(44) all prepared in the presence of carbon pearls.

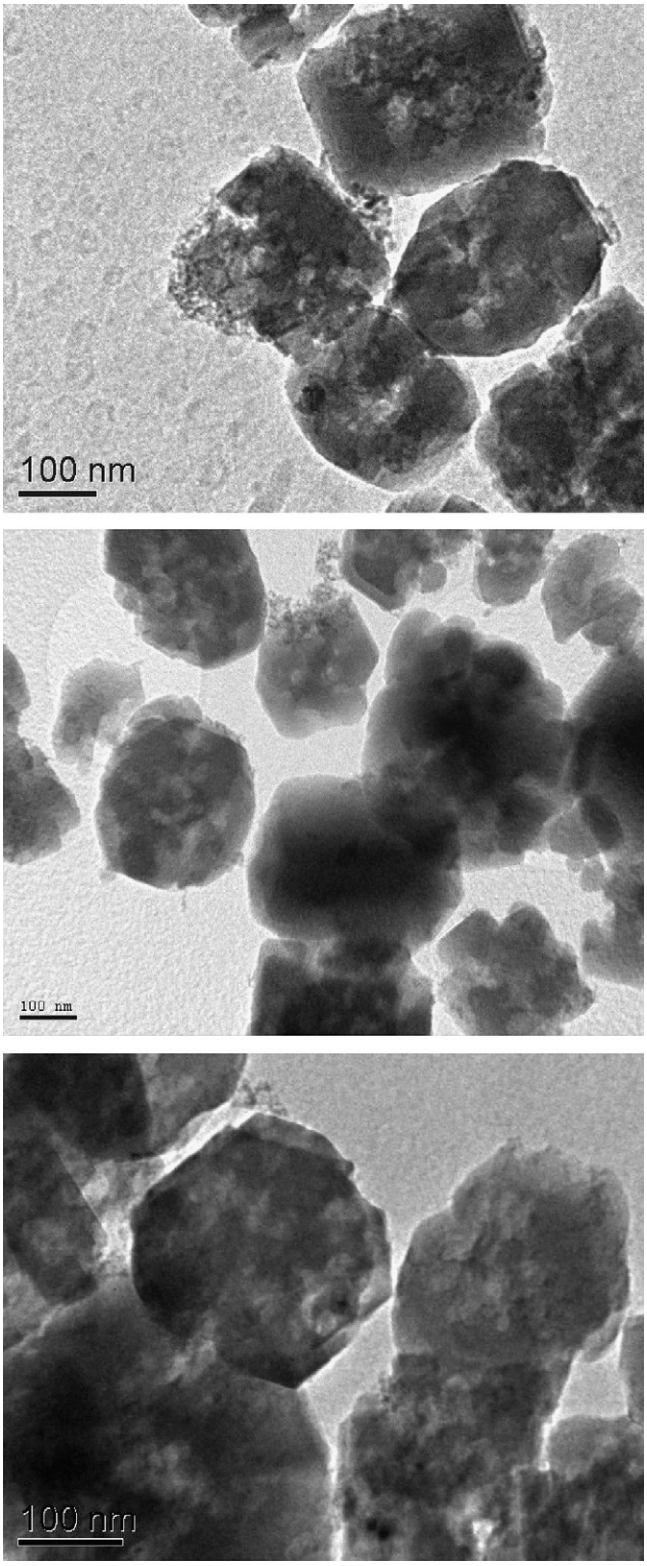

Fig. 3. Representative TEM images of TS-1 prepared via carbon pearls. From top to bottom are PCTS-1(27), PCTS-1(28) and PCTS-1(44).

examined by TEM. Characteristic TEM images are compiled in Fig. 3 for the three examined support materials. The addition of carbon pearls resulted in more irregular crystallite shapes and sizes as compared to morphology of other TS-1 preparation methods presented previously [25]. The crystallites appear to have a rather disruptive, non-continuous external surface as compared to the smooth or cauliflower shaped surfaces generally seen in this laboratory. Though carbon pearls are spheres on the order of 12–20 nm in diameter, there appear to be no specific features of the crystallites that correspond directly to the size and shape of the secondary structure directing agent. Examination of the support material after calcination using SAXS and USAXS found no evidence of void distributions in this size range or long-range ordered mesoporosity. A power law fit to high scattering vector data was consistent with TEM observations in that the particles were more two-dimensional in shape than spherical. The inconsistent shape and particle size of these materials prevented any further quantification of the scattering patterns. Nitrogen adsorption isotherms did not show signs of mesoporosity. The BET surface area, an estimate of the surface area for these microporous materials, and the pore volume were consistent with materials prepared using other synthesis procedures [29,30].

4.2. Kinetic results

The average PO and CO_2 production rates are presented in Figs. 4 and 5 for catalysts 0.03Au/PCTS-1(27), 0.33Au/PCTS-1(28) and 0.04Au/PCTS-1(44) while selectivities and apparent activation energies are presented in Table 2. All catalysts had a stable conversion of propylene throughout the roughly 45-h evaluation period with no evidence of deactivation. The stability of catalyst 0.33Au/TS-1(28) is shown explicitly in Fig. 6. The PO rate is not proportional to either the gold or the titanium content of the catalyst. The most active catalyst, 0.33Au/PCTS-1(28) had a PO rate of 132 $g_{PO}/h/kg_{cat}$ at 200 °C. Despite gold loadings an order of magnitude lower, 0.03Au/TS-1(27) and 0.04Au/PCTS-1(44) produced PO at rates 75 and 50% of that of the most active catalyst. In addition to being the most active catalyst, 0.33Au/PCTS-1(28) also has the highest selectivity to PO, comparable selectivities to CO_2 and lower selectivities to other oxygenates. The apparent energetics for

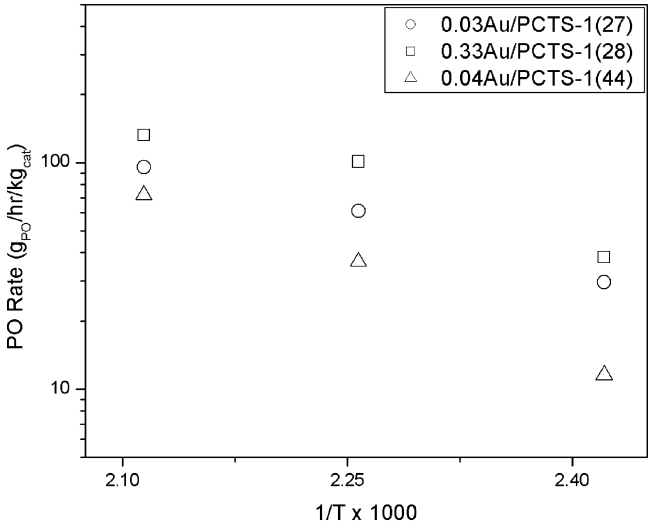

Fig. 4. Normalized PO production rates for catalysts 0.03Au/PCTS-1(27), 0.33Au/PCTS-1(28) and 0.04Au/PCTS-1(44) at 140, 170 and 200 °C.

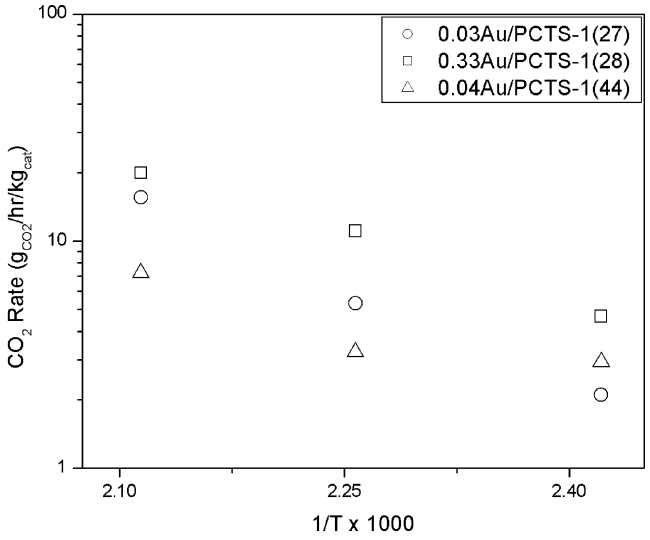

Fig. 5. Normalized CO_2 production rates for catalysts 0.03Au/PCTS-1(27), 0.33Au/PCTS-1(28) and 0.04Au/PCTS-1(44) at 140, 170 and 200 °C.

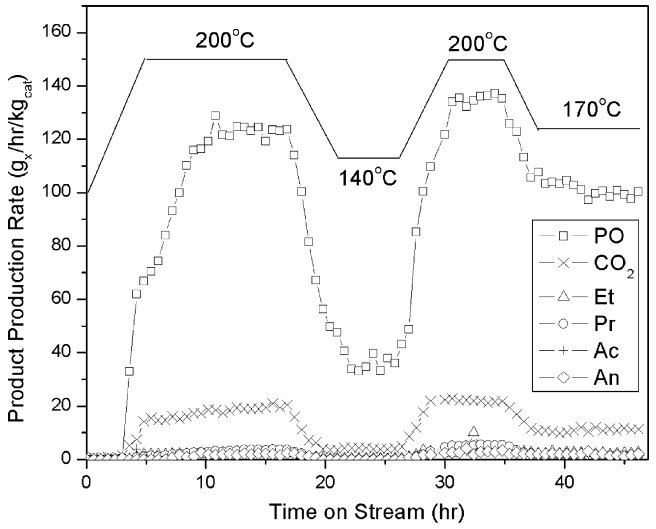

Fig. 6. Normalized production rates for catalyst 0.33Au/TS-1(28) vs. time on stream in hours.

PO formation are roughly similar, though catalyst 0.04Au/TS-1(44) has a higher apparent activation energy than is generally seen over these catalysts. The apparent activation energies for CO_2 formation also differ greatly over these catalysts. Catalyst 0.03Au/PCTS-1(28) has an apparent activation energy to CO_2 that is commonly observed for Au/TS-1 catalysts (∼60 kJ/mol). Catalyst 0.33Au/PCTS-1(28) produces CO_2 far more readily than the other catalysts with an apparent activation much lower than is generally observed. Catalyst 0.04Au/PCTS-1(44), while not producing a large amount of CO_2 on a per gram catalyst basis, has an apparent activation energy that is very low at 24 kJ/mol. This, however, may result from the non-linear relationship shown in Fig. 5 between the log of the rate and inverse absolute temperature.

Both 0.03Au/PCTS-1(27) and 0.04Au/PCTS-1(44) produce propanal far more readily than 0.33Au/PCTS-1(28) and may be a result of low gold loadings. The selectivity to propanal is an order of magnitude higher than that of 0.33Au/PCTS-1(28) while the apparent activation energy to propanal is nearly one-third of the unusually high value of 52 kJ/mol for catalyst 0.33Au/PCTS-1(28). In addition, the low temperature behavior of these catalysts shows a progressive shift in selectivity to propanal at constant propylene conversion. At higher temperatures this shift is not present, perhaps because PO never further reacts to propanal or the isomerization is sufficiently reversible such that any propanal reverts to PO before desorption (Fig. 7).

The hydrogen selectivity (efficiency) for these catalysts, estimated from the oxygen consumption during reaction, was approximately 10 ± 5%. Therefore, a vast majority (∼90%) of the hydrogen converted directly to water and did not contribute to the generation of PO.

Following reaction, all three catalysts were examined by TEM in order to observe any gold particles that formed with time on stream. Only catalyst 0.33Au/PCTS-1(28) possessed observable gold particles (Fig. 8). The average gold particle size obtained from eight TEM micrographs was found to be 3.5 ± 1.4 nm and has been noted in Table 1. Gold particles appear to be concentrated at the edges of the crystallite. More specifically, the gold particles seem to have preferentially anchored at disordered edges and interfaces between support particles. Some support particles appear to have a more crystalline core surrounded by lacy materials, which serve as a preferential anchor point for gold particles.

Table 2
Kinetic data for 0.03Au/PCTS-1(27), 0.33Au/PCTS-1(28) and 0.04Au/PCTS-1(44) at 140, 170 and 200 °C (Et, Ethanal; Pr, Propanal; Ac, Acetone; An, Acrolein)

Catalyst	Temperature (°C)	Selectivity (%)						$E_{a,\ app}$ (kJ/mol)			Rate (g_{PO}/h/kg_{cat})	Conversion (%)
		PO	CO_2	Et	Pr	Ac	An	PO	Pr	CO_2		
0.03Au/PCTS-1(27)	200	77	5.5	2.3	12	1.7	2.1	32	16	54	95	7.7
	170	81	3.1	2.3	11	1.4	1.4				61	4.7
	140	74	2.3	3.1	17	1.8	2.0				30	2.5
0.33Au/PCTS-1(28)	200	87	5.8	1.9	2.6	1.2	1.6	34	52	39	132	9.7
	170	90	4.3	1.9	1.5	1.1	1.7				101	7.2
	140	94	5.1	0.76	0.12	0.25	0.25				38	2.9
0.04Au/PCTS-1(44)	200	77	3.4	2.5	14	1.2	2.4	50	19	24	72	5.9
	170	74	2.9	3.0	16	1.3	3.0				36	1.5
	140	49	5.4	6.8	26	2.1	11				12	3.1

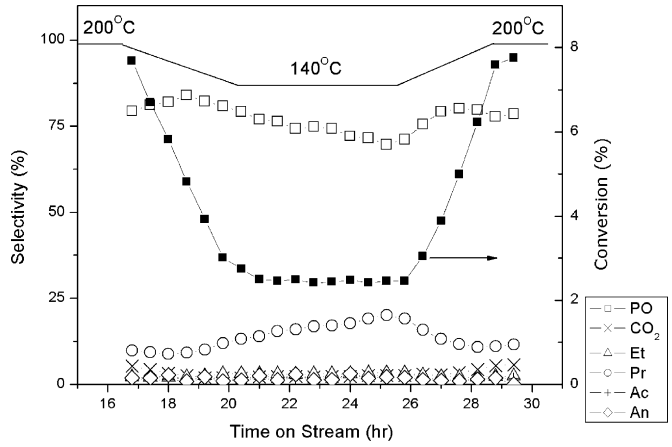

Fig. 7. Low temperature shift in selectivity to propanal of catalyst 0.03Au/TS-1(27) with time on stream.

5. Discussion

A primary assumption of this work is that the crystal structure of TS-1 is capable of supporting an enhanced number of structure defects in proximity to titanium. Despite being well ordered crystal structures, TS-1 and S-1, both generally contain between 5 and 8% silicon vacancies, corresponding to 5–8 vacancies per unit cell [31–34]. With a maximum titanium substitution for silicon of 2% (corresponding to 1–2 Ti atoms per unit cell), the complicated connectivity and symmetry of the MFI-structure makes the positioning of adjacent titanium ions and silicon vacancies more likely than the products of their respective probability distributions would suggest. Given that there are only 12 distinct crystallographic positions within the unit cell, the actual probability of finding a silicon vacancy adjacent to a titanium center would be closer to 8% × 2% × 12%, which raises the likelihood of a titanium/defect pair to around 1 per unit cell. The relatively small number of titanium/defect pairs acting as anchor sites may also be a cause for the apparent intrinsic low gold loadings of the high silicon to titanium TS-1 catalyst and the very limited number of active Au–Ti entities discussed previously [25]. That work shows that gold loading tracks titanium loading but ultimately does not appear to be specifically associated with either the bulk titanium content or that of the external surface. In addition, the incorporation of titanium into the silicalite-1 structure is usually said to have a stabilizing effect since the overall symmetry increases with the shift from monoclinic $P2_1/n$ to orthorhombic *Pnma*, however the addition of the larger Ti^{4+} ion into the framework does impart stress onto the surrounding bonds. Though many Rietveld refinements of powder X-ray and neutron diffraction data in the published literature result in drastically different preferential placements of vacancies and titanium in the zeolite framework [31–34], perhaps the most comprehensive neutron diffraction study [32] did show a high probability of titanium substitution and silicon vacancy at the T1 and T5 sites, which are crystallographically adjacent.

The carbon pearls synthesis was an attempt to enhance these structural defects. Despite the incorporation of a significant volume fraction of carbon pearls into the zeolite growth gel, XRD confirmed that the orthorhombic MFI structure of TS-1 was retained. Though a rough estimate of the degree of structural disorder introduced into the sample could be

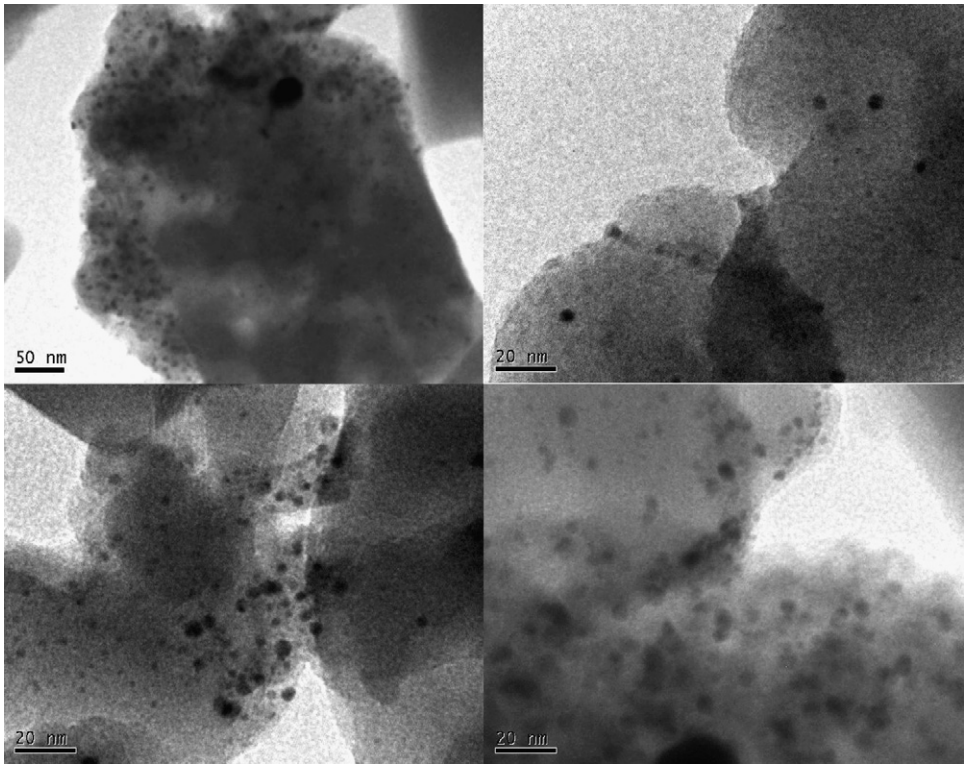

Fig. 8. Representative TEM micrographs showing gold particles on 0.33Au/PCTS-1(28) following 45 h on stream.

expected from the broadening of diffraction peaks, with the exception of PCTS-1(28), none of the samples appears to have a diffraction pattern that has any broader reflections than the support materials examined previously in this laboratory [5,25]. More direct observations of crystal morphology via TEM did show crystallites that were craggier and irregularly shaped than is observed for catalysts prepared by other hydrothermal methods [29,30]. Despite this irregular shape, nitrogen adsorption isotherms, SAXS patterns and USAXS patterns showed no evidence of mesoporosity, especially in the size range of the carbon pearls. The local titanium bonding environment, as shown by DRUV–vis, does not consist of exclusively tetrahedral entities. The additional high wavelength shoulders found in all three DRUV–vis patterns are all consistent with octahedral titanium species of various sizes since the absorptions occur at 240 nm and higher. With the two distinct high wavelength shoulders to the main tetrahedral absorption peak, PCTS-1(27) represents the most impure of the TS-1 samples, indicating two distinct sizes of octahedral titanium contaminants. The higher energy absorption represents the smaller of the octahedral titanium species because of the increase in the ligand to metal charge transfer for titanium as particles of anatase shrink to the nanoscale. Despite this apparently significant impurity, no bulk phase anatase is present since there is no significant adsorption above 350 nm, which would be characteristic of the pure titania polymorph. The impurity of this sample is likely a result of the synthesis method. In this procedure, the zeolitic templating agent was impregnated onto dried carbon pearls and then the silicon and titanium precursors were added in a second impregnation. This two-step impregnation potentially limits interaction between the templating agent and the moisture and air sensitive organic titanium precursor, resulting in the formation of octahedral species prior to the capture and incorporation of titanium into the rigid zeolite framework. The initial intention of this method was to use the carbon pearls as an anchor for the titanium precursor, thus forcing any voids formed by the removal of the carbon pearl to be lined with a titanium-rich surface. As these voids would likely be on the order of 12–20 nm, it was assumed that this would increase the amount of tetrahedral titanium proximate to gold particles too large to access the zeolite pore system. There is no evidence, however, that the titanium remained sited near the carbon pearls following the hydrothermal step of the synthesis. Had all the titanium remained in the vicinity of the carbon pearls, the local environment would have been so saturated with titanium (>2 mol% of the silicon), that a significant fraction of that titanium should exist as extraframework octahedral species. Given that the material still consisted primarily of tetrahedral titania, it seems possible that a significant portion of the titanium eventually worked into the bulk of the gel where it was incorporated into the framework.

Support materials PCTS-1(28) and PCTS-1(44) contained an even higher fraction of tetrahedral titanium. Though there is a significant extraframework octahedral titanium impurity, as evidenced by the high wavelength shoulders on the tetrahedral absorption, it appears far less significant than the octahedral species in PCTS-1(27). The more complete incorporation of titanium into the zeolite framework was likely a result of modifications to the synthesis procedure. The first impregnation of the carbon pearls consisted of the zeolite structure directing agent and the organic titanium precursor followed by impregnation by the organic silicon precursor. The mixing of the titanium precursor and templating agent likely allowed for titanium to be incorporated into the zeolite framework before octahedral titanium species could be formed.

The three catalysts prepared from these support materials were all active and stable for the production of PO, despite having significantly different physical qualities and energetics. The most active catalyst, 0.33Au/PCTS-1(28), captured an order of magnitude more gold from the DP precursor solution than did the other two catalysts. This catalyst, following reaction, was the only one to show any gold particles. Careful examination of the number of TEM micrographs showed that the gold particles were concentrated on defective surfaces, particle interfaces and lacy material attached to more well-defined crystallites. This, in combination with the fact that gold deposits far more efficiently on extended titanium phases such as anatase surfaces, would imply that the gold preferentially deposited on extraframework species. Although this explanation does not appear consistent with the high amount of extraframework titanium species and an equivalent amount of defective surfaces and lacy material as observed by TEM on the 0.03Au/PCTS-1(27) catalyst, this formulation is the most likely to have that Ti encapsulated in the interior of the crystallites and, thus, inaccessible to the gold. During the deposition of gold, catalysts 0.03Au/PCTS-1(27) and 0.04Au/PCTS-1(44) behaved more like the very active catalysts presented previously by this laboratory [25], in which only a very small percentage (<2%) of the available gold in the precursor solution was deposited on the support surface.

In spite of relatively drastic differences in metal loading and preparation method, all three catalysts produced PO at similar rates. The primary differences appeared in the energetics of the reaction. Both 0.03Au/PCTS-1(27) and 0.33Au/PCTS-1(44) had similar apparent activation energies to PO of 32 and 34 kJ/mol, respectively, which are within the range of 22–40 kJ/mol generally observed for Au/TS-1 catalysts. Despite similar energetics in the production of PO, the energetics for CO_2 formation differs significantly over these catalysts. Catalyst 0.03Au/PCTS-1(27) had an apparent activation energy for complete combustion of 54 kJ/mol, which is consistent for catalysts of the Au/TS-1 system. Catalyst 0.33Au/PCTS-1(28) had an apparent combustion activation energy of 39 kJ/mol, which is very low for catalysts of this type but may be a result of the high gold loading and the considerable number of gold particles observable after reaction. A low apparent activation energy and low rate to CO_2 would both suggest a limited number of CO_2 sites, perhaps implying that high gold loadings are capable of blocking sites that normally result in complete combustion. The energetics of catalyst 0.04Au/PCTS-1(44) are significantly different than have been observed for Au/TS-1 catalysts in this laboratory. The apparent activation energy for PO is very high at 50 kJ/mol and the apparent activation energy for complete combustion is very low at 24 kJ/mol. There is no

simple explanation for the high apparent activation for PO production. If desorption of PO plays a dominant effect in the energetics of the system [1,11], it is conceivable the introduction of carbon pearls in the synthesis mixture could have produced a catalyst that made PO desorption more energetically demanding. The low combustion apparent activation energy is more easily explained using Fig. 5. The temperature program used for the evaluation of these catalysts began at 200 °C and then proceeded to 140, 200 and finally 170 °C. The fact that the average CO_2 production rate at 140 and 170 °C is nearly the same and that CO_2 production is presumably lower than expected implies that some combustion sites were eliminated most likely during the high temperature cycle (200 °C). It is not inconceivable that combustion sites were blocked by partial oxygenates at low temperature and that these intermediates could have been further decomposed at higher temperatures resulting in deactivation of the site. There was no commensurate effect on PO production. However, it has been shown previously [25] that PO and CO_2 producing sites do not directly interconvert.

The most dramatic differences between the three examined catalysts were in the production of side products. While the catalysts produced similar absolute amounts of PO and CO_2, catalysts 0.03Au/PCTS-1(27) and 0.04Au/PCTS-1(44) produced significantly more propanal and the apparent activation energy to propanal was much lower over these catalysts than for the most active catalyst, 0.33Au/PCTS-1(28). As discussed previously [7,8], propanal production is generally attributed to the acid-catalyzed ring opening of PO over the catalyst surface. There is no obvious source of acidity over these catalysts. While there is a significant octahedral titanium contamination of these support materials, the selectivities to PO degradation products and acrolein are similar to those of catalysts evaluated previously in this laboratory [25]. Though extraframework species are generally considered detrimental to activity and selectivity, they appear to have no significant effect in these materials, potentially because the octahedral species are not accessible from reaction surfaces and may have somehow been encapsulated during the zeolite synthesis. In addition, extraframework titania species would be expected to be amphoteric, thus there should be a relationship between increased propanal production and the base catalyzed ring opening of PO to form acetone. There does not appear to be such a relation for the catalysts examined. Even more anomalous than the high selectivity to propanal is the progressive conversion of PO at low temperature (140 °C) to propanal over catalysts 0.03Au/PCTS-1(27) and 0.04Au/PCTS-1(44) shown in Fig. 7. Despite constant propylene conversion, it appears that some acidic character is developing on the catalyst surface resulting in the monotonic increase in propanal production at the expense of PO. Even more intriguing is the observation that this acidic quality does not appear to affect product rates or selectivity at high temperatures since both quantities appear nearly identical at both 200 °C portions of the reaction cycle.

Despite the complexities revealed in the analysis of these catalysts, the manipulation of support morphology using carbon pearls did result in the most active catalysts yet reported. Catalyst 0.33Au/PCTS-1(28), with a PO rate of 132 $g_{PO}/h/kg_{cat}$ at 200 °C, exceeds the previously best published rates of 93 $g_{PO}/h/kg_{cat}$ at the lower temperature of 160 °C produced over gold on a amorphous mesoporous titanosilicate by Haruta and co-workers [24] and slightly exceeds the best catalyst previously prepared in this laboratory (116 $g_{PO}/h/kg_{cat}$ at 200 °C) [25]. Catalyst 0.33Au/PCTS-1(28) retains the superior stability of Au/TS-1-based catalysts produced in this laboratory with steady PO production for over 45 h on stream. On a per gram gold basis, though, this catalyst produces PO at only 40 $g_{PO}/h/g_{Au}$, implying that not all the gold on this catalyst is being efficiently utilized for the production of PO. Despite the large number of gold particles, in the appropriate size range suggested by literature of 2–5 nm, there is not a substantial increase in activity over previous best catalysts produced in this laboratory (0.05 wt% Au on TS-1(Si/Ti = 36)). In addition, the considerable activity of the other catalysts examined with gold loadings an order of magnitude lower, still implies that observable gold entities may not be the only seat of catalytic activity in this system.

The truly remarkable quality of catalyst 0.33Au/TS-1(28) is that the PO production rate is high and the stability is remarkable in spite of the number of detrimental characteristics of the catalyst. A gold loading of 0.33 wt% on TS-1 is sufficiently high to lead one to expect deactivation due to gold agglomeration [5]. There is also no excessive combustion activity as would be expected for catalysts with high gold loadings and average particle sizes greater than 2 nm [1]. In addition, the support material has a considerable octahedral Ti concentration that would be expected to hamper stability and result in increased combustion activity. Perhaps the high gold loading deposited more selectively on the octahedral titanium species and served to eliminate non-selective oxidation sites through poisoning by carbon deposition and PO polymerization [6,8] or by sufficiently high gold loadings so as to produce inactive metal surfaces. It is also possible that silica encapsulated the octahedral species. In any case, these support materials have shown a remarkable robustness in the production of PO despite properties that have severely hampered to activity and stability of other catalysts.

6. Conclusions

Carbon pearls were used to disrupt the morphology of TS-1 support materials by disrupting crystallite formation during hydrothermal synthesis. This synthesis technique did result in TS-1 as confirmed by XRD and produced crystallites with complex morphology as viewed using TEM. Despite containing significant amounts of octahedral titanium impurities, catalysts made from these supports had high activity and selectivity implying that the synthesis of these materials may have resulted in encapsulation of octahedral titanium species so as to prevent their interaction with catalytically active surfaces. This synthesis method resulted in catalysts with stable PO production in excess of 45 h on stream at temperatures ranging from 140 to 200 °C and more specifically, the most active catalyst of the Au–Ti system with a PO production rate of

132 $g_{PO}/h/kg_{cat}$ at 200 °C. Despite this high activity, this catalyst (0.33Au/PCTS-1(28)) had a PO production rate per gram Au of only 40 $g_{PO}/h/g_{Au}$ implying that large number of gold entities visible by TEM may not account for the entirety of the epoxidation activity of the Au–Ti system.

Acknowledgements

Support for this research was provided by the United States Department of Energy, Office of Basic Energy Sciences through Grant number DE-FG02-01ER-15107. The authors would also like to thank Prof. Mark E. Davis, for bringing our attention to the work of the Haldor-Topsøe Company on carbon-modified TS-1.

References

[1] T. Hayashi, K. Tanaka, M. Haruta, J. Catal. 178 (1998) 566.
[2] E.E. Stangland, K.B. Stavens, R.P. Andres, W.N. Delgass, Stud. Surf. Sci. Catal. 130 (2000) 827.
[3] E.E. Stangland, K.B. Stavens, R.P. Andres, W.N. Delgass, J. Catal. 191 (2000) 332.
[4] E.E. Stangland, B. Taylor, R.P. Andres, W.N. Delgass, J. Phys. Chem. B 109 (2005) 2321.
[5] N. Yap, R.P. Andres, W.N. Delgass, J. Catal. 226 (2004) 156.
[6] G. Mul, A. Zwijnenburg, B. van der Linden, M. Makkee, J.A. Moulijn, J. Catal. 201 (2001) 128.
[7] B.S. Uphade, S. Tsubota, T. Hayashi, M. Haruta, Chem. Lett. (1998) 1277.
[8] T.A. Nijhuis, B.J. Huizinga, M. Makkee, J.A. Moulijn, Indust. Eng. Chem. Res. 38 (1999) 884.
[9] M.G. Clerici, G. Bellussi, U. Romano, J. Catal. 129 (1991) 159.
[10] M. Haruta, M. Date, Appl. Catal. A 222 (2001) 427.
[11] C. Qi, T. Akita, M. Okumura, M. Haruta, Appl. Catal. A 218 (2001) 81–89.
[12] S. Tsubota, D.A.H. Cunningham, Y. Bando, M. Haruta, Stud. Surf. Sci. Catal. 91 (1995) 227.
[13] Y.A. Kalvachev, T. Hayashi, S. Tsubota, M. Haruta, Stud. Surf. Sci. Catal. 110 (1997) 965.
[14] M. Haruta, B.S. Uphade, S. Tsubota, A. Miyamoto, Res. Chem. Intermed. 24 (1998) 329.
[15] Y.A. Kalvachev, T. Hayashi, S. Tsubota, M. Haruta, J. Catal. 186 (1999) 228.
[16] B.S. Uphade, M. Okumura, S. Tsubota, M. Haruta, Appl. Catal. A 190 (2000) 43.
[17] B.S. Uphade, M. Okumura, N. Yamada, S. Tsubota, M. Haruta, Stud. Surf. Sci. Catal. 130 (2000) 833.
[18] B.S. Uphade, Y. Yamada, T. Akita, T. Nakamura, M. Haruta, Appl. Catal. A 215 (2001) 137.
[19] B.S. Uphade, T. Akita, T. Nakamura, M. Haruta, J. Catal. 209 (2002) 331.
[20] A. Zwijnenburg, A. Goossens, W.G. Sloof, M.W.J. Crajé, A.M. van der Kraan, L.J. de Jongh, M. Makkee, J.A. Moulijn, J. Phys. Chem. B 106 (2002) 9853.
[21] A.K. Sinha, S. Seelan, T. Akita, S. Tsubota, M. Haruta, Appl. Catal. A 240 (2003) 243.
[22] C. Qi, T. Akita, M. Okumura, K. Kuraoka, M. Haruta, Appl. Catal. A 253 (2003) 75.
[23] C. Qi, M. Okumura, T. Akita, M. Haruta, Appl. Catal. A 263 (2004) 19.
[24] A.K. Sinha, S. Seelan, S. Tsubota, M. Haruta, Angew. Chem. 43 (2004) 1546.
[25] B. Taylor, J. Lauterbach, W.N. Delgass, Appl. Catal. A: Gen. 291 (2005) 188.
[26] D.H. Wells, W.N. Delgass, K.T. Thomson, J. Am. Chem. Soc. 126 (2004) 2956.
[27] C.J.H. Jacobsen, C. Madsen, J. Houzvicka, I. Schmidt, A. Carlsson, J. Am. Chem. Soc. 122 (2000) 7116.
[28] I. Schmidt, A. Krogh, K. Wienberg, A. Carlsson, M. Brorson, C.J.H. Jacobsen, Chem. Commun. (2000) 2157–2158.
[29] M. Taramasso, G. Perego, B. Notari, U.S. Patent 4,410,501 (1983).
[30] R.B. Khomane, D.B. Kulkarni, A. Paraskar, S.R. Sainkar, Mater. Chem. Phys. 76 (2002) 227.
[31] C. Lamberti, S. Bordiga, A. Zecchina, A. Carati, A.N. Fitch, G. Artioli, G. Petrini, M. Salvalaggio, G.L. Marra, J. Catal. 183 (1999) 222.
[32] P.F. Henry, M.T. Weller, C.C. Wilson, J. Phys. Chem. B 105 (2001) 7452.
[33] C. Lamberti, S. Bordiga, A. Zecchina, G. Artioli, G. Marra, G. Spano, J. Am. Chem. Soc. 123 (2001) 2204.
[34] C.A. Hijar, R.M. Jacubinas, J. Eckert, N.J. Henson, P.J. Hay, K.C. Ott, J. Phys. Chem. B 104 (2000) 12157.